

**Kumaran Kolandaivelu<sup>a)</sup>**

Harvard-MIT Division of Health Science  
and Technology,  
Massachusetts Institute of Technology,  
77 Massachusetts Ave. Bldg 16-343,  
Cambridge, MA 02139

**Elazer R. Edelman**

Harvard-MIT Division of Health Science  
and Technology,  
Massachusetts Institute of Technology,  
77 Massachusetts Ave. Bld 16-343  
Cambridge, MA 02139;  
Cardiovascular Division,  
Department of Medicine,  
Brigham and Women's Hospital,  
Harvard Medical School, 75 Francis St.,  
Boston, MA 02115

# Low Background, Pulsatile, In Vitro Flow Circuit for Modeling Coronary Implant Thrombosis

*We have developed an in vitro method for creating pulsatile flows to mimic coronary type flow patterns on a beat-to-beat basis. The flow is created by accelerating fluid loops about an axis, inducing relative wall motion. Using this technique, a variety of oscillating flow patterns can be generated and modulated. Such flow generation offers the potential to monitor sensitive, flow-dependent, biological parameters like thrombosis while minimizing background disturbances from pump action and circuit effects. We examined this potential by measuring the loop occlusion time for loops stented with stainless steel 7-9 NIR® stents and stentless control loops. [DOI: 10.1115/1.1517062]*

## Introduction

Biocompatibility has been a major issue in the clinical use of prosthetic implants. One such set of applications includes prostheses such as endoluminal stents or vascular grafts that allow blood to flow beyond a previously stenosed arterial segment. When such a foreign structure comes into contact with tissue and blood, a variety of biological consequences ensue. Reactions ranging from thrombosis, to inflammation, to restenosis, can result in acute or long-term device failure. The thrombotic reaction is one of the earliest responses to implantation and by virtue of its rapid acceleration and potential for complete luminal occlusion, one of the most devastating. Current implantation techniques and drug therapies have limited the incidence of acute and subacute occlusion to around 5%, with the outcome of such events often being fatal due to their unexpected, sudden onset [1,2]. Moreover, mural thrombosis isolated to the wall of the blood vessel is likely the inciting and promoting event for all subsequent events. The developing clot not only serves as a scaffold for the in growth of migrating and proliferating cells, but as a source and reservoir for chemical mediators of these cellular events [3]. Such cellular proliferation leads to pathological restenosis in 20-50% of cases and is dependent on factors such as vessel size, lesion complexity, and stent design [4]. Accordingly, elucidation and control of the thrombotic process is especially important for the continued use and development of vascular implants.

Vascular patency relies on a careful balance of chemical mediators and local fluid dynamics. Disturbances, even as simple as the insertion of a small intravascular wire, can cause profound micro-environmental changes that alter blood flow and coagulability. A thrombus develops and propagates when the stimulatory forces cannot be balanced by the regulatory measures as fibrin, activated from precursor fibrinogen, stabilizes a mass of aggregating platelets.

One difficulty that has limited the extensive examination of bioprosthetic thrombosis is the highly flow-dependent nature of thrombosis and lack of widely applicable flow models. Flow can affect the components of thrombosis either through physical shear dependent mechanisms, such as von Willebrand's Factor dependent

platelet activation, or through the mass transport of cellular and molecular substances into and out of a given region [5-7]. Thus, control and documentation of reproducible flows are essential to the study of the dynamically coupled cellular and protein pathways leading to implant thrombosis.

We sought to develop a system that created controllable, coronary-like flow conditions (as determined by various dimensionless parameters), while reducing the background levels of thrombosis by minimizing the length, volume and discontinuities of a tubing loop into which a prosthetic device could be placed. The loop was filled with the desired blood constituents and spun about its axis in a prescribed and controlled fashion to modulate the inertial flow of the contained fluid through transmitted shear forces from the tubing wall, thereby generating relative flow.

As a test of the mechanical suitability of the system, we created and measured various flow profiles (impulse, square, triangular, sinusoidal, coronary) in a fluid loop run under the nominal geometric and fluidic conditions found in an adult left anterior descending coronary branch. A preliminary study to assess the system's ability to investigate coronary arterial implant thrombosis was performed on polished, stainless steel 7-9 NIR® stents. These trials indicated the system's utility in assessing occlusion time as a rough measure of thrombotic potential. We also showed the sufficiently low background levels in stentless, control circuits—a requisite for future, sensitive, inter-prosthetic studies to be performed.

## Methods

**Flow Theory.** To create the desired flow profiles, a fluid-filled torus was rotated about its axis. When impulsively started, there is inertial fluid motion relative to the toroid wall. The fluid accelerates primarily due to momentum transfer into the bulk fluid via shear forces. When the loop is accelerated, there continues to be relative motion, and hence relative flow. Lyne has previously analogized such fluid motion to pressure driven flows where, moving in a reference frame with the wall, the acceleration takes on the driving character of a body force [8]. Analytical solutions of straight tube models of oscillatory wall flow derived elsewhere directly show such a pressure gradient/wall acceleration symmetry on the development of radial velocity gradients [9-12]. While the absolute fluid velocity in an inertial reference frame may change under pressure driven or accelerating wall conditions, it is the maintenance of the velocity gradients, or shear, that is important in the flow-dependent thrombotic reactions [5-7]. Rather than

<sup>a)</sup>Corresponding author: Kumaran Kolandaivelu, Division of Health Science and Technology, Massachusetts Institute of Technology, Bldg 16-343, 77 Massachusetts Avenue, Cambridge, MA 02139. Phone: (617)252-1655 Fax: (617)253-2514 E-mail: kkolanda@excite.com

Contributed by the Bioengineering Division for publication in the JOURNAL OF BIOMECHANICAL ENGINEERING. Manuscript received April 2001; revised manuscript received June 2002. Associate Editor: A. P. Yoganathan.

**Table 1** List of the dimensionless parameters considered, along with customary definitions and typical values found in the left anterior descending coronary branch (LAD) [13].  $V_{\text{fluid}}$  is the mean cross-sectional axial velocity of the fluid,  $\nu$  is the kinematic viscosity,  $\omega$  is the flow oscillatory frequency,  $a$  is the vessel radius, and  $R$  is the radius of curvature of the loop.  $\Psi$  This value for  $\kappa_{\text{peak}}$  was calculated assuming a peak  $\text{Re}$  of twice the  $\bar{\text{Re}}$  and an aspect ratio,  $R/a$ , of 10 as suggested by Chang and Tarbell [14].

Dimensionless #	Definition	Typical Coronary Values (LAD)
Mean Reynolds # ( $\bar{\text{Re}}$ )	$\frac{2a\bar{V}_{\text{fluid}}}{\nu}$	$153 \pm 64$
Wormersely # ( $\alpha$ )	$\alpha\sqrt{\omega/\nu}$	$1.5 \pm 0.27$
Peak Dean # ( $\kappa_{\text{peak}}$ )	$\text{Max}\left(\frac{2aV_{\text{fluid}}}{\nu}\sqrt{a/R}\right)$	$95^{\Psi}$

fluid being conducted to and from a reactive wall surface, the relevant reaction control volumes are conducted away from the lagging fluid.

Since this manner of flow generation requires acceleration, and net positive flow requires a net positive acceleration, impractically large loop angular velocities can result. However, the physiological coronary flow pattern is pulsatile, comprising a diastolic, high flow phase and a systolic, low flow phase where the flow can drop to zero, or even briefly reverse. Thus, two options exist for producing coronary-like flows: introduction of a one-way valve or creating bi-directional flow. Although the one-way valve could be employed for certain applications, its physical presence and the imposed water-hammer effect when the fluid is jerked to a halt could increase the circuit's background levels of thrombosis. Bi-directional flow at one half the frequency ( $\omega_{\text{system}}$ ) of the desired heart rate ( $\omega_{\text{coronary}}$ ) can be established by following each loop acceleration profile with a symmetric deceleration. For the purposes of this study, bi-directionality was deemed a suitable solution so long as the oscillatory frequency was kept low enough to ensure minimal flow before the next pulse began.

Using such a technique, we hoped to create time-varying flows whose characteristics, as defined by the dimensionless mean Reynolds ( $\bar{\text{Re}}$ ), based on an absolute velocity, and Wormesley ( $\alpha$ ) numbers were typical of coronary flows, as well as estimate the secondary flow effects of curvature by considering the peak Dean number ( $\kappa_{\text{peak}}$ ) associated with our system (see Table 1).

Table 1 defines these conventional dimensionless parameters [15]. In each of these parameters, a Newtonian approximation for  $\nu$  is used, as has been shown to be valid for high shear conditions ( $>100\text{s}^{-1}$ ) and often applied when considering coronary flow [9,14,16,17]. However, the customary definition of  $\kappa$  is not applicable in the rotating toroid case, as the relevant velocity term must take into account the fluid's axial velocity in an inertial reference frame ( $V_{\text{fluid}}$ ) which gives rise to the centrifugal forces, and a different wall velocity ( $V_{\text{wall}}$ ). It is the difference in these components that gives rise to the relative wall velocity ( $V_{\text{rel}}$ ) and hence, the centrifugal pressure mismatch leading to secondary flows.

To determine a modified  $\kappa_{\text{peak}}$  number ( $\kappa'_{\text{peak}}$ ) for comparison with the nominal conditions of Table 1, we can consider the definition of  $\kappa$  as a ratio of the square root of the product of the secondary flow inertial and centrifugal forces to the viscous forces [15], where

$$\text{Inertial forces} \rightarrow \frac{\rho V_{\text{secondary}}}{2a} \quad (1)$$

$$\text{Centrifugal forces} \rightarrow \frac{\rho(|V_{\text{fluid}}^2 - V_{\text{wall}}^2|)}{2R} \quad (2)$$

$$\text{Viscous forces} \rightarrow \frac{\mu V_{\text{secondary}}}{(2a)^2} \quad (3)$$

which have been determined from an order of magnitude consideration of the relevant quantities [18]. In these equations,  $V_{\text{secondary}}$  represents a typical secondary fluid velocity,  $\rho$  is the density of the fluid,  $\mu$  is the dynamic viscosity of the fluid. The use of tube and loop diameters ( $2a$ ,  $2R$ ) rather than radii have been used to allow reduction into a quantitatively proper form as conventionally used. The differential term in the centrifugal relation accounts for the relative centripetal motions in an inertial frame. When both motions are present,  $\kappa'_{\text{peak}}$  becomes

$$\kappa'_{\text{peak}} = \text{Max}\left(\left[\frac{2a(|V_{\text{fluid}}^2 - V_{\text{wall}}^2|)^{1/2}}{\nu}\right]\left[\frac{a}{R}\right]^{1/2}\right) \quad (4)$$

where  $\nu$ , is given by the ratio  $\mu/\rho$ . When  $V_{\text{wall}}$  is zero, as in the case of forced flow through a curved, stationary pipe,  $\kappa'_{\text{peak}}$  reduces to the standard form given in Table 1.

**System Design.** The key components of the system include fluid loops, rotor-stages, a driving motor, a motion controller, a measurement system and an incubator (Fig. 1). The blood and prosthetic device were placed into the fluid loop. This loop was then fit onto a rotor stage and placed in axial alignment with other loops to be tested under the same flow conditions. The entire rotor system was driven through a desired oscillating motion profile via the motor and controller system. This motion created the bi-

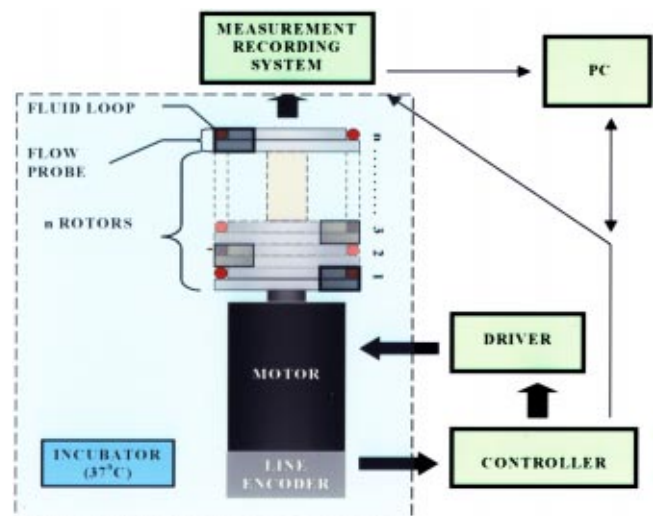


**Fig. 1** General system schematic

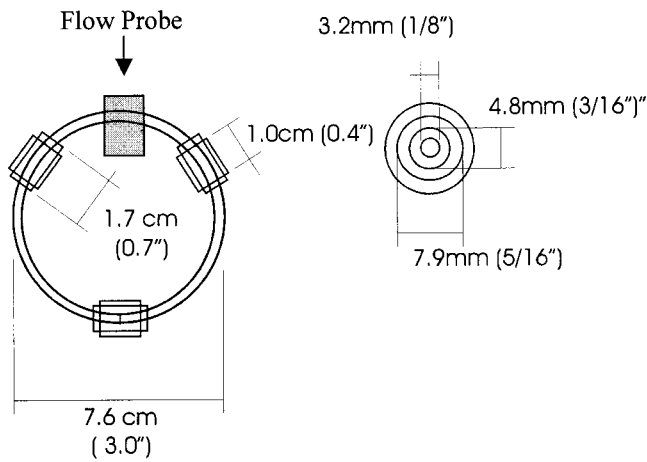


**Fig. 2 Embodied fluid loop design and dimensions; (a) Fluid loop; (b) cross-sectional view through a fitting. The three equally spaced fittings were positioned to minimally disrupt the loop curvature. One fitting serves as a connector to create the fluid loop by securely holding the two ends of the tubing length in apposition. The two other fittings serve as inlet and outlet ports for the injection of fluid.**

directional flows that were measured via onboard, extracorporeal flow probes built into the rotor stages. The rotating system was maintained at 37°C in an incubator and connected remotely to the controller circuitry and flow recorder stationed externally at room temperature.

In the current embodiment, the 7.6 cm (3.0") diameter fluid loops are made from a 24.0 cm (9.5") length of 3.2 mm ID/4.8 mm OD (1/8" ID/3/16" OD) S-50-HL Tygon® tubing (Fig. 2)

approximating the geometric conditions (both ID and R/a ratio) found in the adult coronary artery [13]. To form the fluid loops, the ends of the tubes were square cut with the axial dimension and placed in apposition. This connection was held via an overlapping segment of 4.8 mm ID/7.9 mm OD (3/16" ID / 5/16" OD) S-50-HL Tygon® tubing. Further compressive support was provided by an elastic sleeve made from Silastic® silicon tubing placed over the joiner segment of tygon. Two similar structures were slid onto the loop at equally spaced 120-degree intervals to cause the least deviation in toroid curvature possible. The two additional sleeves serve as outlet and inlet ports for the replacement of the loop's contained air by the desired fluid. Filling was accomplished via a syringe whose hypodermic needle tip was slid under the outer most elastic sleeve and pushed through the middle sleeve and inner loop layers. Small-bore needles were used to create the smallest possible disturbance to the loop's luminal surface. A 26-gauge needle was used at one of the ports for the evacuation of air. As a compromise between the need for a small injection port and an atraumatic injection of cellular components, a 20-gauge needle was used for the transfer of blood products.

The rotors are the modular discoid platforms that hold the fluid loops. Each was manufactured out of a stock of delrin plastic. The key features of the rotors are a grooved resting stage to hold the fluid loop, a keyed axial hole for rotor stacking and alignment, a chiral notch for the placement of the flow transducer, and a slot through which the transducer connections are passed. The notch chirality allows sequential rotors to be stacked with the probes facing opposite directions in order to minimize asymmetrical loading. With the current rotor system's shaft, 6 rotor stages can be stacked, along with a cap structure that serves as a location for on-board instrumentation. A centered hole allows for axial coupling to the motor.

The driving motor is an Electro-Craft® E643 DC servo-brush motor (peak torque 0.16 Nm (720 oz in); peak operating speed 4800 RPM). The required parameters were estimated from a

straight tube, Newtonian fluid approximation for oscillatory flow, as used by Moore Jr. et al. [9], which was augmented by an impedance factor as suggested by Chang and Tarbell [14] to account for curvature effects [10,15].

The components of the motor control system integrate readily and allow for the generation of specific flow profiles. These components include a Renco RM15 Encoder, an Electro-Craft® IQ-550 Position Control Module, an Electro-Craft® Max-100 PWM Servo Drive, and a Windows compatible PC terminal running IQ Master software (Fig. 1).

To measure the loop flow rates, Transonic 3CA flow probe leads are connected to a specially constructed junction on each rotor stage. Upon stacking, the male connector junction on a given rotor stage allows communication with the female junction on the stage immediately below it. Thus, each stacked rotor was hard-wired to all of the probes. This design allows the stages to be modular for loading and possible future expansion, with the top most stage relaying all probe signals to the on-board probe multiplexer. These signals were passed sequentially to a Transonic T106 Flow meter that outputs a voltage signal, recordable on a computer via a National Instruments® LAB-PC A/D interface and LABTECH Version 8.1 software package (Laboratory Technologies Corporation ©). The trigger to sequentially switch probes was provided by the high to low or low to high state change of a digital output pin on the IQ 550 controller. This switch was programmed to occur after each flow cycle, or beat. In this method, all of the probes' signals were merged into a continuous waveform. A final signal was sent from the multiplexer to the computer encoding a specific probe label. Therefore, with the waveform and corresponding probe label information, an individual fluid loop could be monitored throughout the time course of an experiment.

An 8 lead rotary electrical coupling interfaces the rotating loop reference frame with the inertial frame. The onboard multiplexer probe output was wired to four of the rotary couplings. Two additional couplings provide power (+10V,GND) to the multiplexer. The last two lines provide contacts for the probe switch trigger and the probe label. Although this system can monitor and record the full flow profiles in the fluid loops, only the peak flow values were stored to disk in actual loop occlusion time experiments to reduce the amount of data storage. These peaks effectively convey information on change in the fluidity of the blood.

**Performance Testing.** To demonstrate the range of system capabilities, a single fluid loop was filled with a 6:4 water/glycerol mix to match the Newtonian approximation blood viscosity under arterial flow conditions ( $0.04 \text{ cm}^2 \text{ s}^{-1}$ ) [16] and placed on a rotor stage. Subsequently, the rotor was driven through a variety of motion profiles to generate impulse, square, triangle, sinusoidal, and coronary-type flows. The full flow profiles, rather than just peak data, were recorded via the LABTECH software.

To assess the system's potential in studying prosthetic thrombosis, both a source of blood and a prototypical implant were needed. In this preliminary study, surplus American Red Cross blood products were used to obtain quantities sufficient to allow several experiments to be performed on the same batch of blood for precision testing. Fresh frozen plasma and fresh platelet concentrates (both anticoagulated with 10mmol citrate) were utilized as these contained the key ingredients of classical thrombosis, neglecting the red and white blood cells in this first level of study. Type AB+ fresh frozen plasma (FFP) with a prescribed storage life of 6 months post-collection was stored at -20°C. The plasma was thawed in a 37°C water bath for 45 minutes and then spun down at 10000 G to eliminate debris such as preformed platelet microvesicles. The supernatant was filtered 4 times through a 0.2 μm low protein binding filter to further ensure clean FFP. The platelets (type AB+ PRP) were obtained within one day of collection and stored on a 70 RPM rocker at 22°C. These were used within the first two days post-collection as was justified from adequate functional comparisons with freshly drawn volunteer platelets.

One hour before a planned experiment, the platelets were added to the FFP at a constant ratio of 1:4 PRP to FFP and returned to the rocker for equilibration. Each loop required 2.5 ml of the FFP/platelet mix to ensure proper filling. To reduce experimental error from mixing and handling variation, the total volume of the suspension for a given run (15 ml) was pooled and prepared in a single tube.

Polished, passivated, 7-9 stainless steel NIR® endovascular stents were obtained from Medinol Ltd. (Jerusalem, ISRAEL). While the platelets were equilibrating in the filtered FFP, the stents were expanded 1 cm from the end of the tygon tubing via a 36mm Maxxum™ 3.5 SCIMED® balloon catheter under a pressure of 12 atm. The tubes were closed into their loop format ensuring a gapless fit. When the plasma/platelet mix was ready, 5M Ca2+ was added to bring the sample to an additional 10mmol Ca2+ concentration, negating the citrate's anticoagulant chelating effect. The stented loops were then filled with the plasma/platelet mix as described above and placed onto the rotors. This process was sequentially performed as rapidly as possible (~15 sec/loop) while ensuring safe handling of the blood components and proper filling of the tubes. Once complete, the rotors were placed onto the rotor shaft and spun according to the desired motion profile within the 37°C incubator. Background thrombosis was assessed by running three stented loops against three stentless control loops.

## Results

**Mechanical validation.** The impulsive response of the system was examined after a brief burst of torque was supplied to the rotor. Some points to note in this profile (Fig. 3) are the 0-135 ml/min rise time of 0.1 sec and a decay time constant of 0.1 sec. These values help characterize the realistic impulse function achievable with the current setup, which serves as the limiting building block from which other functions can be composed. Some examples (square, triangular, sine waves) of other possible flows are shown in Fig. 4(a-c). Here, the periodic, bi-directional nature of the flow is evident. Again, this type of oscillation is necessary in the methodology used to create flow, as no valves were present in the circuit.

Since we hope to investigate coronary arterial events, a coronary flow pattern [19] (scaled to a 60 beat/sec frequency) was approximated with our bi-directional model as shown in Fig. 5a. Figure 5b gives the driving wall velocities,  $V_{wall}$ , required to achieve the coronary-type flow,  $V_{rel}$ , and the derived absolute fluid velocity in the inertial frame,  $V_{fluid}$ . This simulated coronary-type flow is characterized by a  $\overline{Re}$  of 150 (based on  $|V_{rel}|$ ), an  $\alpha$  of 2 (based on a  $\omega_{coronary}$ ), and a  $\kappa'_{peak}$  of 135 (as defined by equation 1).  $\overline{Re}$  and  $\alpha$ , when compared with Table 1, indicate the ability to achieve coronary-type principle flows, while keeping secondary flow effects (as estimated by  $\kappa'_{peak}$ ) to within physiological levels.

The pliability of the system allows principle wave characteristics such as frequency and amplitude to be readily varied accord-

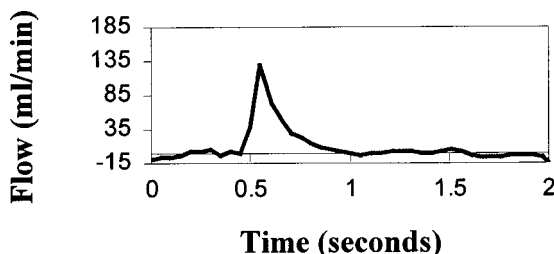


Fig. 3 Impulsive fluidic response to a step in rotor velocity

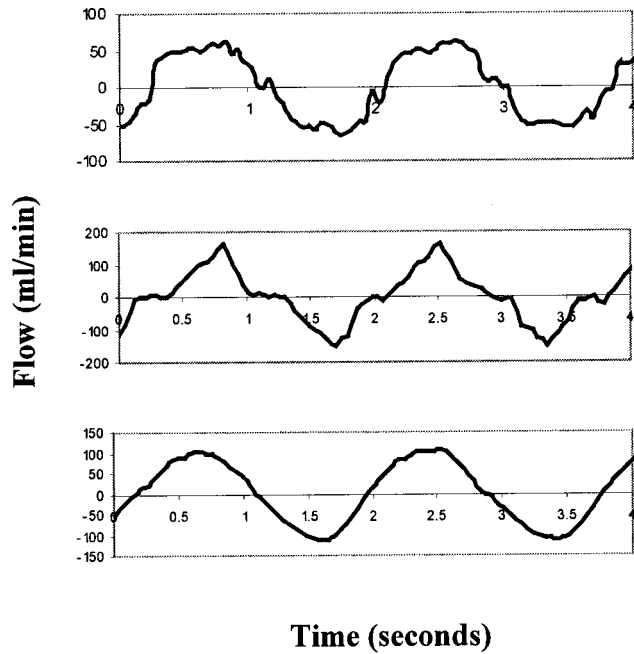


Fig. 4 Sample flow profiles depicting some of the possibilities achievable with this type of flow generation; (a) Square; (b) Triangular; (c) Sinusoidal

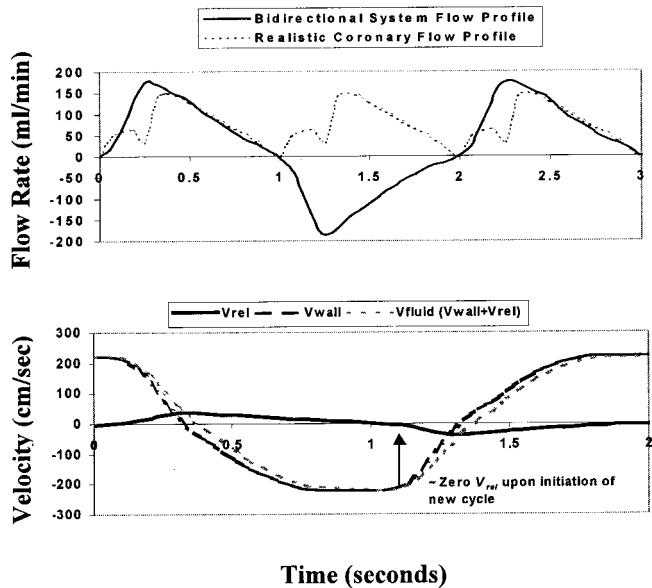


Fig. 5 Modeled coronary profiles; (a) Typical left anterior descending coronary flow pattern superimposed on the modeled, bi-directional, coronary-type flow profile; (b) The wall,  $V_{wall}$ , and fluid,  $V_{fluid}$ , velocities in the inertial reference frame required to drive the relative coronary flow velocity,  $V_{rel}$ . Note that  $V_{rel}$  is essentially zero by the time  $V_{wall}$  initiates a new cycle.

ing to the experimental protocol. Furthermore, the system allows for tailoring of more detailed parameters such as the systolic:diastolic ratio if desired.

**Feasibility for Coagulation Testing.** As a preliminary test, six stents were positioned in their respective fluid loops and run through the described coronary flow protocol. The results obtained after parsing the data according to the probe label and running a

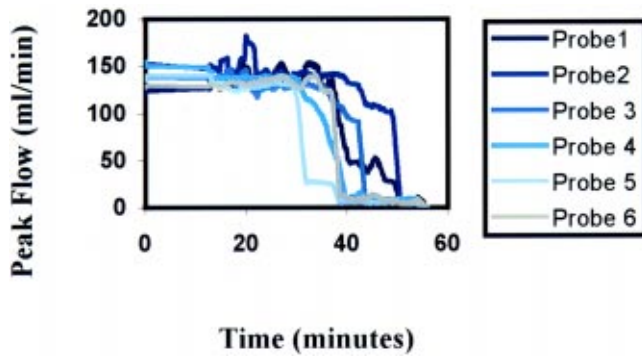


Fig. 6 Occlusion time trial for 6 stainless steel 7-9 NIR® stented loops

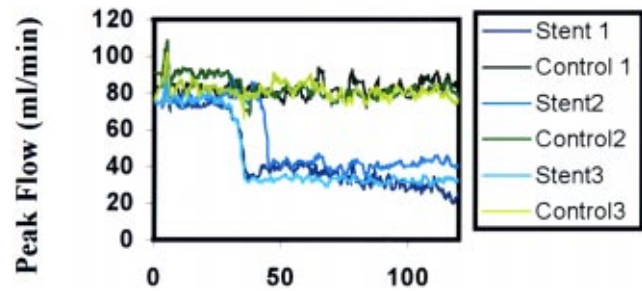


Fig. 7 Occlusion time trial depicting 3 stainless steel 7-9 NIR® stented loops (in blue) and 3 stainless steel control loops (in green)

5-point moving average demonstrate an initial constant flow rate followed by a fairly rapid drop to zero flow (Fig. 6). The actual initial flows in each loop are identical as they have the same dimensions, fluid properties, and driving motion profiles. Variation in the measured start-up flow rates arises from the hard-wire calibration of the meter for a specific flow probe's (#1's) signal while our system employs six different probe signals. To correct this, each signal can be re-calibrated according to these initial deviations where identical fluid conditions are known to exist. The drop-off point indicates when the thrombus is occluding the stent. If a zero-flow condition is taken as the end point, the average occlusion time for this run is  $43.1 \pm 6.8$  min.

Another initial test of the system is to compare a trial of three stented tubes to three empty control tubes. The transformed peak flow data for such a run is given in Fig. 7. As above, the initial flow period followed by a drop-off is witnessed in the stented samples, with an average clotting time of  $39.1 \pm 1.7$  min. The stentless controls remained patent for the +2 hour duration of the test.

## Discussion

Along with the relevant biological factors, the physical environment needs to be considered when investigating physiological phenomena. Indeed, when dealing with complex reaction networks such as the thrombotic or inflammatory responses, flow has been shown to be critical in determining outcomes [20]. Various flow systems have been developed to study the thrombotic process and though they have contributed greatly to our understanding of vascular biology, many of these systems have limitations.

Loops, partially filled with blood, can be mounted on a tilted turntable. As the table spins, gravity keeps the fluid at the bottom of the tube, creating flow [21,22]. However, the partial filling creates a large air/fluid interface leading to protein aggregation and denaturation, resulting in a departure from the physiological situation. Furthermore, this method does not allow for arterial

flow profiles to be obtained. Parallel-plate flow chambers enable microscopic visualization of surface-cellular interactions in real time, but cannot readily be applied to clinical devices and physiological geometries [23,24]. Other flow systems have been created to examine real devices but they often employ roller or peristaltic pumps to drive blood through long in vitro circuits [25,26]. High background levels of thrombosis can result from the large surface area of peristaltic tubing, the multiple components and discontinuities of the system, and the roller pump's action. Such noise can be reduced by using sub-physiological flow rates, though this raises concern as to the adequacy of modeling highly flow dependent phenomenon [27]. Some of these issues can be avoided in systems that funnel blood directly from a human into a length of tubing where the stent is placed [28]. This reduces the background noise by allowing a minimal tubing length and eliminating peristaltic action, though the signal is likewise reduced from the single pass over the stent. Additionally, this setup does not allow for controllable flow rates.

Animal in-vivo and ex-vivo models recreate physiological flows and have been used to show various differences in stent thrombosis [29,30]. However, these are limited to studies involving parameters that can be controlled in animals. Extraneous variables may also be amplified in these in-vivo systems, while interspecimen variation creates additional uncertainty [31]. Furthermore, the use of such animals, like clinical trials [1,2,32–34] is restrictive and should likely be reserved until extensive and definitive in vitro evaluations have been completed.

The principle goal of this work has been to develop an in-vitro model of the in-vivo flow situation to aid in the study of vascular phenomenon such as thrombosis. The proposed design is a system that minimizes background sources of thrombosis in a flow circuit where the axial  $Re$  and  $\alpha$  were matched to typical coronary values found in the literature. This was accomplished by rotating fluid-filled loops in a prescribed fashion to create inertially driven flows.

Restrictions on the obtainable flow patterns were given by the realistic impulse function whose dynamics were not instantaneous. The finite rise time was a result of the limitations of rotor inertia, friction, and peak obtainable torque. If a quicker response is required, these parameters can be changed. The decay time constant on the other hand, being a function of the vessel radius and kinematic fluid viscosity, is not subject to change. Therefore, relative flows decaying to nearly zero ( $<2\%$  peak) in times less than 4 time constants are not possible without flow reversal. Figure 5b shows that this flow resetting is possible for the coronary-like flow conditions considered, as the relative flow velocity is approximately zero by the time the wall velocity begins to initiate a new pulse.

While the relative flow essentially resets to zero initial conditions after each uni-directional beat, we must point out that the created flows are bi-directional in nature. While many of the thrombotic protein and cellular surface reactions have been shown to be dependent on shear, which we attempt to approximate by matching beat-to-beat dimensionless parameters, the potential influences of bi-directionality on factors such as mass transport (which has been shown to be dependent on flow oscillation) [6] and cellular function (adhesion and activation) [35] may need to be considered.

Another aspect of the flow that is altered is the secondary flow. Physiologically, such flows have been shown to be up to 5% of the axial flow velocity, shifting the peak of the velocity contour towards the outer wall via half-tube, single vortex flows. However, peak wall shear rates due to these flows can be up to 40% of the peak axial wall shear rates [14]. While precise determination of these secondary flow fields through numerical simulation would be interesting and of value in finding the exact time-dependent wall shear rates, we have found that the magnitude of the secondary flows in our system (as determined by  $\kappa'_{peak}$ ) are comparable to those found in a coronary setting of similar axial

flows. Qualitatively, a deviation in the secondary flow pattern results from a disconnect between the centrifugal force and the relative wall velocity (which are normally linked in stationary wall flows). During part of the cycle, the bulk fluid velocity is greater than the wall-boundary layer velocity, as is generally the case [14]. However, in our rotational system, there are also times when the wall-boundary layer velocity is greater than the bulk fluid's, resulting in a counter-rotating secondary flow drive. Considering these effects, we see that we can minimize the secondary flows as well as maintain beat-to-beat symmetry by using a zero DC component of  $V_{\text{wall}}$ . For further reduction in these flows, a larger  $R/a$  ratio can be used.

Another point that should be mentioned is the lack of documentation of the hydrostatic pressures within our system. While a pressure head can be maintained within our closed loops, we relied primarily on our blood injection technique for consistency. This seemed reasonable as absolute pressures have been found to have only subtle effects on blood under physiological conditions, with relevant changes occurring in more extreme situations such as those associated with diving or hyperbaric chambers [36]. However, we must keep in mind that a cyclic, radial wall stretch does not occur with our system and this could be relevant should the actions of endothelial or smooth muscle cells be incorporated into the model [37].

As a preliminary biological test of the embodied, bi-directional system, the occlusion time of polished, passivated, 7-9 stainless steel NIR® stents was assessed by performing trials on stented loops. In these trials, the peak flow data show an essentially binary phenomenon, characterized by an initial flow rate that quickly dropped to zero as the thrombus occluded the circuit with an average clotting time of 43.1 +/- 6.8 min. As a measure of background thrombosis, stentless control tubes were run against stented loops. These control loops remained unoccluded for the duration of the trials, indicating the sufficiently low levels of background thrombosis, while the stented loops clotted after 39.1 +/- 1.7 min.

The approximate 40-minute stent occlusion times are phenomenological findings that occur in our in-vitro system. In-vivo, thrombotic occlusion occurs at a much lower rate and generally takes place subacutely over the course of several days. There are various potential explanations for such observational discrepancies. The clinical situation has both innate and external counter measures, such as a reactive endothelial layer and drug therapies that help to regulate thrombosis. Indeed, with the advent of suitable drug regimes and implantation technique, the thrombosis rate has dropped from nearly 25% in initial studies to its current low levels (<5%) [2]. Furthermore, our system is a closed, in-vitro model where produced substances are not cleared. This could not only help to explain the regularity of clotting seen within our system, but also the fairly rapid drop to zero flow as the confined reactions could augment rapidly due to positive feedback processes.

Due to such differences between our model and the physiological situation, we hope not to study the physical occurrence of end-state occlusion for a given stent-type (though this is an important preliminary observation), but the comparative differences between stent-types in the factors leading up to thrombosis. Such differences are important not only in overt stent occlusion, but the sub-clinical levels of thrombosis that play a more general role in the overall prosthetic response.

The current results give insight into the important characteristics of the system's precision and background noise levels. Maximizing precision and minimizing background noise allows for effective inter-prostheses studies. Investigations are currently being performed to assess such inter-stent differences, both on the bases of occlusion times, as well as more detailed platelet and coagulation studies. Using the highly adjustable nature of the setup, we hope to also investigate how these various factors interact with endovascular prosthesis in different flow regimes.

While the current application of the described flow system is to study intravascular thrombosis, its use can be generalized to other situations where a carefully controlled, pulsatile flow is required with adjustments (loop dimensions, surface properties, uni/bi-directional flow) being made to suit the different requirements. Such a system would hopefully be of use in helping to better bridge the experimental gap existent between the in-vitro and in-vivo environments.

## Acknowledgments

This work was supported in part by grants from the National Institutes of Health (GM/HL 49039 and HL 60407) and an Established Investigator award to ERE from the American Heart Association.

## References

- [1] Schatz, R. A., 1997, "The Evolution of Antithrombotic Therapy in Coronary Stenting," *American Heart Journal*, **134**, pp. S78-S80.
- [2] Mak, K., Belli, G., Ellis, S. G., and Moliterno, D. J., 1996, "Subacute stent thrombosis: Evolving issues and current concepts," *J. Am. Coll. Cardiol.*, **27**(2), pp. 494-503.
- [3] Waugh, J. M., Li-Hawkins, J., Yuksel, E., Kuo, M. D., Cifra, P. N., Hilfiker, P. R., Geske, R., Chawla, M., Thomas, J., Shenaq, S. M., Dake, M. D., and Woo, S. L. 2000, "Thrombomodulin overexpression to limit neointima formation," *Circulation*, **102**(3), pp. 332-337.
- [4] Kastrati, A., Mehilli, J., Dirschinger, J., Pache, J., Ulm, K., Schuhlen, H., Seyfarth, M., Schmitt, C., Blasini, R., Neumann, F. J., and Schomig, A., 2001, "Restenosis after coronary placement of various stent types," *Am. J. Cardiol.*, **87**(1), pp. 34-39.
- [5] Lascalzo, J., and Schafer, A.I., 1994, *Thrombosis and Hemorrhage*, Blackwell Scientific Publications.
- [6] Basmadjian, D., 1990, "The effect of flow and mass transport in thrombogenesis," *Ann. Biomed. Eng.*, **18**, pp. 685-709.
- [7] Turitto, V. T., and Baumgartner, H. R., 1975, "Platelet deposition on subendothelial exposed to flowing blood: Mathematical analysis of physical parameters," *Trans. Am. Soc. Artif. Intern. Organs*, **21**, pp. 593-601.
- [8] Lyne, W. H., 1970, "Unsteady viscous flow in a curved pipe," *J. Fluid Mech.*, **45**(1), pp. 13-31.
- [9] Moore, Jr. J. E., Guggenheim, N., Delfino, A., Doriot, P. A., Dorsaz, P. A., Rutishauser, W., and Meister, J. J., 1994, "Preliminary analysis of the effects of blood vessel movement on blood flow patterns in the coronary arteries," *J. Biomech. Eng.*, **116**, pp. 302-306.
- [10] Brodkey, R. S., 1967, *The Phenomena of Fluid Motions*, Addison-Wesley Publishing Company.
- [11] Zapryanov, Z., and Matakiev, V., 1980, "An exact solution of the problem of unsteady fully-developed viscous flow in slightly curved porous tube," *Arch. Mech.*, **32**, pp. 461-474.
- [12] Myers, L. J., and Capper, W. L., 2001, "Analytical solution for Pulsatile Axial Flow Velocity Waveforms in Curved Elastic Tubes," *IEEE Trans. Biomed. Eng.*, **48**(8), pp. 864-873.
- [13] Nerem, R. M., and Seed, W. A., 1983, "Coronary Artery Geometry and its Fluid Mechanical Implications," *Fluid Dynamics as a Localizing Factor in Atherosclerosis*. (Edited by Schettler, G.). Springer, Berlin.
- [14] Chang, L. J., and Tarbell, J. M., 1988, "A numerical study of flow in curved tubes simulating coronary arteries," *J. Biomech.*, **21**, pp. 927-937.
- [15] Berger, S. A., Talbot, L., and Yao, L.-S., 1983, "Flow in curved pipes," *Annu. Rev. Fluid Mech.*, **15**, pp. 461-512.
- [16] Perktold, K., Nerem, R. M., and Peter, R. O., 1991, "A numerical calculation of flow in a curved tube model of the left main coronary artery," *J. Biomech.*, **24**(3/4), pp. 175-189.
- [17] Perktold, K., Hofer, M., Rappitsch, G., Loew, M., Kuban, B. D., and Friedman, M. H., 1998, "Validated computation of physiologic flow in a realistic coronary artery branch," *J. Biomech.*, **31**, pp. 217-228.
- [18] Rosenhead, L., 1963, *Laminar Boundary Layers*, Oxford University Press.
- [19] Berne, R. M., and Levy, M. N., 1992, *Cardiovascular Physiology (Sixth Ed.)*, Mosby Year Book.
- [20] Baldwin, S., and Basmadjian, D., 1994, "A mathematical model of thrombin production in blood coagulation: The sparsely covered membrane case," *Ann. Biomed. Eng.*, **22**, pp. 357-370.
- [21] Chandler, A. B., 1958, "In vitro thrombotic coagulation of the blood," *Lab. Invest.* **7**(2), pp. 110-114.
- [22] Haycox, C. L., and Ratner, B. D., 1993, "In vitro platelet interactions in whole human blood exposed to biomaterial surfaces: Insights on blood compatibility," *J. Biomed. Mater. Res.*, **27**, pp. 1181-1193.
- [23] Grabowski, E. F., 1988, "Effects of contrast media on erythrocyte and platelet interactions with endothelial cell monolayers exposed to flowing blood," *Invest. Radiol.*, **23**(Suppl 2), pp. S351-S358.
- [24] Goto, S., and Handa, S., 1998, "Coronary thrombosis: Effects of blood flow on the mechanism of thrombus formation," *Jpn. Heart J.*, **39**(5), pp. 579-596.
- [25] Beythian, C., Terres, W., and Hamm, C. W., 1994, "In vitro model to test the thrombogenicity of coronary stents," *Thromb. Res.*, **75**(6), pp. 581-590.

- [26] Gutensohn, K., Beythian, C., Bau, J., Meinertz, T., and Kuehnl, P., 1997, "Flow cytometric analysis of coronary stent-induced alterations of platelet antigens in an in vitro model," *Thromb. Res.*, **86**(1), pp. 49–56.
- [27] Beythien, C., Gutensohn, K., and Bau, J., 1999, "Influence of stent length and heparin coating on platelet activation: A flow cytometric analysis in a pulsed floating model," *Thromb. Res.*, **94**, pp. 79–86.
- [28] Tarnok, A., Mahnke, A., Muller, M., and Zotz, R. J., 1999, "Rapid in vitro biocompatibility assay of endovascular stents by flow cytometry using platelet activation and platelet-leukocyte aggregation," *Cytometry*, **38**, pp. 30–39.
- [29] Makkar, R. R., Eigler, N. L., Kaul, S., Frimmerman, A., Nakamura, M., Shah, P. K., Forrester, J. S., Herbert, J. M., and Litvack, F., 1998, "Effects of clopidogrel, aspirin, and combined therapy in a porcine ex-vivo model of high-shear induced stent thrombosis," *Eur. Heart J.*, **19**(10), pp. 1538–1546.
- [30] Verheye, S., Markou, C. P., Salame, M. Y., Wan, B., King, 3rd S. B., Robinson, K. A., Chronos, N. A., and Hanson, S. R., 2000, "Reduced thrombus formation by hyaluronic acid coating of endovascular device," *Arterioscler., Thromb., Vasc. Biol.*, **20**(4), pp. 1168–1172.
- [31] Schmidt, B., 1994, "Experimental test systems for the assessment of the blood compatibility of materials used in extracorporeal circuits," *Nephrology Dialysis Transplantation*, **9**(Suppl. 2), pp. 77–82.
- [32] Schatz, R. A., Baim, D. S., Leon, M., Ellis, S. G., Goldberg, S., Hirschfeld, J. W., Cleman, M. W., Cabin, H. S., Walker, C., Stagg, J., Buchbinder, M., Teirstein, P. S., Topol, E. J., Savage, M., Perez, J. A., Curry, R. C., Whitworth, H., Sousa, J. E., Tio, F., Almagor, Y., Ponder, R., Penn, I. M., Leonard, B., Levine, S. L., Fish, R. D., and Palmaz, J. C., 1991, "Clinical experience with the Palmaz-Schatz coronary stent: initial results of a multicenter study," *Circulation*, **83**, pp. 148–161.
- [33] Shaknovich, A., Moses, J. W., Bailey, S., Ricci, D., Kiesz, S., Tierstein, P., and Schatz, R. A., 1994, "Subacute stent thrombosis in the stent REStenosis study (STRESS): Clinical impact and predictive factors," *Circulation*, **90**(Suppl 1), pp. I–650.
- [34] De Servi, S., Repetto, S., Klugmann, S., Bossi, I., Colombo, A., Piva, R., Giommi, L., Bartorelli, A., Fontanelli, A., Mariani, G., and Klersy, C., 1999, "Stent thrombosis: Incidence and related factors in the R.I.S.E. Registry (Registro Impianto Stent Endocoronarico)," *Catheterization and Cardiovascular Interventions*, **46**, pp. 13–18.
- [35] Savage, B., Saldivar, E., and Ruggeri, Z. M., 1996, "Initiation of platelet adhesion by arrest onto fibrinogen or translocation on von Willebrand Factor," *Cell*, **84**, pp. 289–297.
- [36] Barshtein, G., Bergelson, L., Gratton, E., and Yedgar, S., 1997, "Membrane lipid order of human red blood cells is altered by physiological levels of hydrostatic pressure," *Am. J. Physiol.*, **272**(1pt2), H538–H543.
- [37] Ziegler, T., and Nerem, R. M., 1994, "Tissue engineering a blood vessel: regulation of vascular biology by mechanical stresses," *J. Cell Biol.*, **56**(2), pp. 147–149.